CHAPTER 6

FINITE ELEMENT ANALYSIS OF MODEL TESTS

6.1 General

The use of Finite Element Analysis (FEA) has become very important in geotechnical engineering because soil behaves in complex and unpredictable ways. Soils show non-linear stress-strain behavior, vary from place to place, and often change over time, which makes it difficult to predict how they will perform under different conditions. Traditional laboratory tests and field investigations, although useful, sometimes, cannot fully reproduce the complicated conditions found in real-life projects, especially for structures like retaining walls, embankments, and foundations. In addition, carrying out large-scale field tests can be expensive and difficult to manage. For these reasons, numerical methods especially the Finite Element Method (FEM) have become reliable and widely used tools for solving difficult geotechnical problems. FEM makes it possible to closely study stress patterns, ground movements, and how the soil interacts with structures in a virtual, controlled environment. However, to be confident in the results from these computer models, it is important to check and confirm them by comparing them with actual model test results or data collected from the field. In this study, results from physical embankment model tests are used to verify the predictions from the finite element analysis, and the comparison of these results is discussed in this chapter.

The validated numerical models not only enhance the understanding of soil-structure interaction mechanisms but also provide a reliable basis for predicting the performance of embankments under various loading and boundary conditions. In the following section, the details of the numerical tool, material properties, and the

procedures adopted for the numerical modeling of single column soil bed and embankment model tests are presented. This is followed by a description of the finite element modeling approach, including the selection of constitutive models, boundary conditions, and mesh configurations employed in the numerical analysis. PLAXIS 3D Version 2021.01.00479 has been used to carry out the numerical analysis.

6.2 PLAXIS 3D software

The finite element method (FEM) is a widely recognized numerical analysis technique used in civil engineering to address complex real-world problems. FEM has been applied in engineering for over last few decades, and among the various software options available, PLAXIS is the most commonly used for geotechnical applications. PLAXIS is available in two versions: PLAXIS 2D and PLAXIS 3D. PLAXIS 3D is a three-dimensional finite element software designed for geotechnical, mining, tunnelling, and rock mechanics applications. It is particularly effective for analyzing deformation, stability, and groundwater flow, and is known for its ability to accurately calibrate material models.

In this study, PLAXIS 3D was used to model the behavior of granular column and soft clayey soil surrounding the column. The software can analyze non-homogeneous and anisotropic materials with nonlinear stress-strain behavior and complex boundaries. The use of finite element numerical tools has been extensively done to analyze the several geotechnical phenomena such as the development of stresses and deformations in foundation systems, embankments, consolidation behavior of soil under structures, pore pressure distributions (Murugesan and Rajagopal 2006; Ambily and Gandhi 2007; Castro and Sagaseta 2009; Shahu and Reddy 2011). Three-dimensional finite element analyses were conducted for single and group of granular columns in this chapter.

6.3 Finite Element Simulation of model tests on single column

This study modeled the constitutive behavior of a granular column reinforced soft clay bed using PLAXIS 3D software. All the components in the model test, namely soft clay, sand mat and granular columns, were modeled using quadratic 10-node tetrahedral elements. The model test tank of 0.3 m x 0.3 m x 0.5 m used in the experimental work was numerically modeled. The lateral boundaries allowed for vertical displacement but restricted horizontal movement. Movement in both the vertical and horizontal directions is restricted on the bottom boundary. In the meantime, the model domain's top surface is free to move vertically in response to applied loads. The results obtained from the finite element analysis are compared with the results of model tests to ascertain the column deformation behavior and the stresses developed in the columns. The initial vertical stress due to gravity load has been considered in the analysis.

Mohr-Coulomb elastoplastic failure criteria were used to model the sand mat, clay bed, and granular column materials, which is consistent with the studies conducted in the past (Ambily and Gandhi 2007; Yoo 2010; Ghazavi and Nazari Afshar 2013). Geogrid encasement material was modeled as an elastic material (Debnath and Dey 2017; Shahu et al. 2023). The material properties used as input in the FEM modeling are listed in Table 6.1.

Deformation controlled loading of the soil bed was adopted for the numerical model. The permeability of the clay bed is very low, which is why an undrained condition was adopted for the soil (Ali et al. 2014; Shahu et al. 2023). Drained behavior was adopted for the stone aggregates and plastic granules. Experimentally determined values of shear strength were used for the soft soil. The elastic modulus of the soft soil was obtained through the oedometer test for a Poisson's ratio of 0.49; this was adopted as per the typical value suggested by Plaxis software for short-term material behavior

for undrained C conditions. Similar values of poisson's ratio were adopted for clay under undrained loading condition in previous studies (Hasan and Samadhiya 2017; Pradeep and Kumar 2023) . The elastic modulus values for sand and granular materials were obtained from triaxial tests performed in the lab. The Poisons ratio of 0.3 was adopted, as suggested by Bowles (1996). The deformation at the interface of the column and soil is mainly in the form of bulging, and negligible shear displacement takes place; thus, no interface elements were modeled. The model parameters that are mentioned in Table 6.1, such as the angle of internal friction, modulus of elasticity, and undrained shear strength were determined from relevant laboratory tests. The systematic process of the numerical modeling adopted in this study is presented in Fig. 6.1. The process involved creating soil volumes, defining material properties depicted in Fig. 6.1 (a) and (b). Furthermore, the components of the soft soil foundation system discussed in the experimental study section are discretized by appropriately meshing the geometry as shown in Fig. 6.1 (c) and (d).

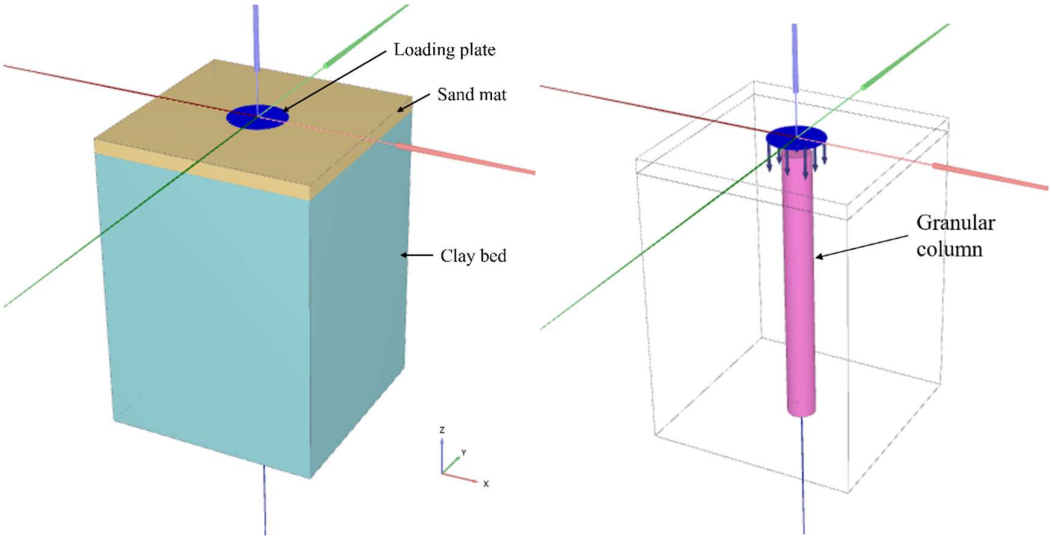

(a) (b)

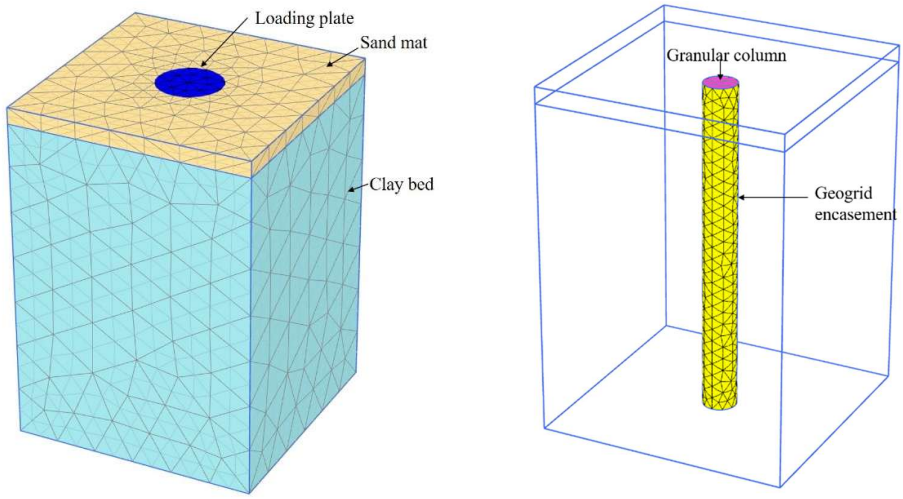

(c) (d)

Fig. 6.1 Process of 3D FEM modeling (a) numerical model of the physical model, (b) single granular column in the soft clay, (c) discretized mesh of the soil bed, (d) meshing of encased granular column.

Table 6.1 Material properties used for finite element analysis.

Parameters	Materials			
	Clay	Sand	Stone aggregates	Plastic granules
Modulus of elasticity (kPa)	1100-3000	20000	45000	30000
Shear strength, c_u (kPa)	5-15	0	0	0
Poisson's ratio, (ν)	0.49	0.3	0.3	0.3
Angle of internal friction, (ϕ^o)	0	36	45	43
Dilation angle (ψ^o)	0	6	15	13

Mesh sensitivity analyses were carried out to check the convergence of the finite element results. Five meshing options, from 'very coarse' to 'very fine' are offered

based on their mesh coarseness factor. The model test components were discretized using a medium mesh discretization. Figs. 6.2 to 6.6 display the mesh discretization available in PLAXIS 3D for modeling the test bed, ranging from very coarse to very fine. Fig. 6.7 displays the mesh convergence study for all mesh discretizations. It can be seen that medium meshing gave satisfactory results compared to fine and very fine mesh. Therefore, medium meshing was selected for embankment modeling as it gave acceptable accuracy with minimum computational cost.

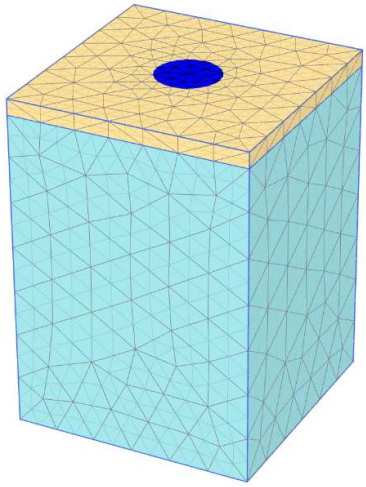

Fig. 6.2 Very coarse meshing adopted for GC improved soft soil ground.

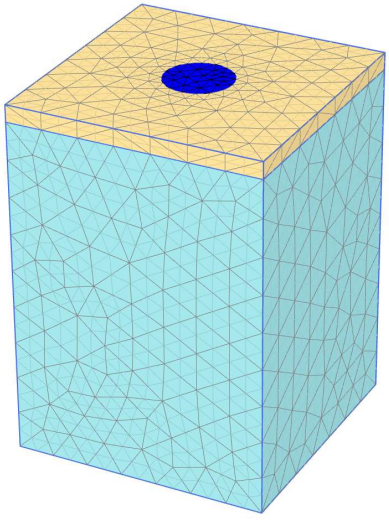

Fig. 6.3 Coarse meshing adopted for GC improved soft soil ground.

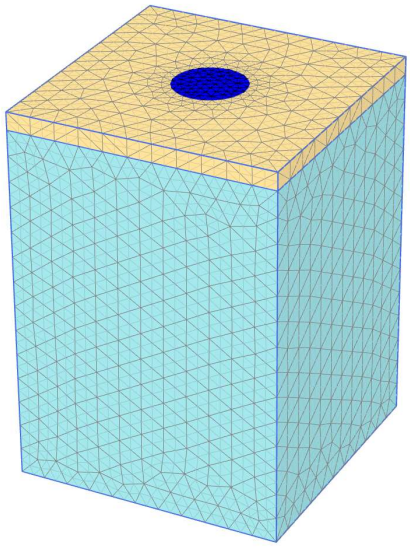

Fig. 6.4 Medium meshing adopted for GC improved soft soil ground.

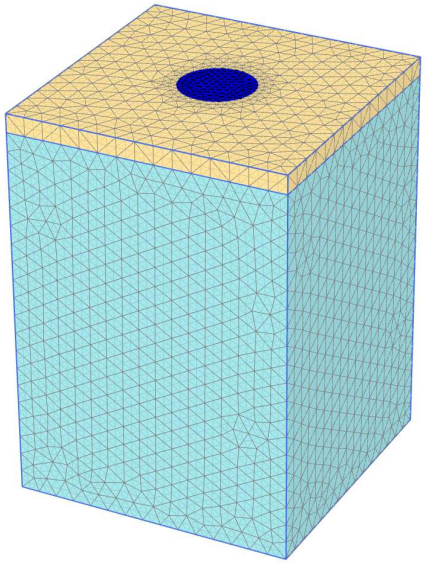

Fig. 6.5 Fine meshing adopted for GC improved soft soil ground.

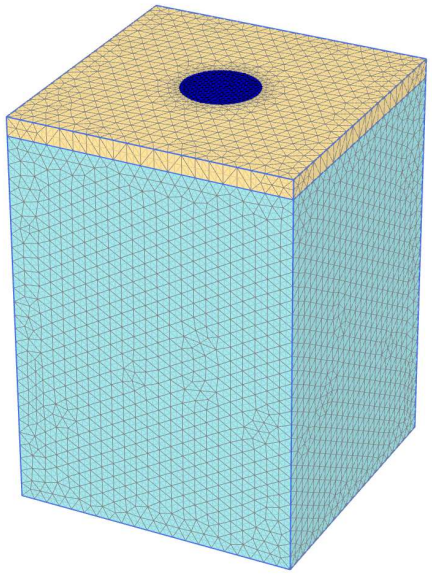

Fig. 6.6 Very fine meshing adopted for GC improved soft soil ground.

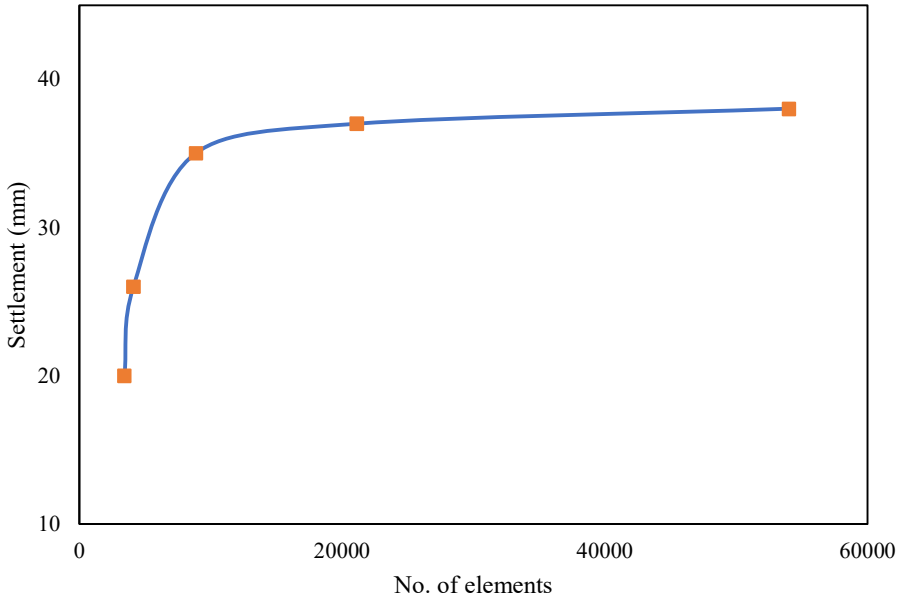

Fig. 6.7 Mesh convergence analysis of FEM modeling of single column in Plaxis 3D.

Table 6.2 provides information on the total number of elements and nodes utilized in discretizing various components of the selected finite element meshes for a GC-reinforced soft soil.

Table 6.2 Details of mesh diagnostics in finite element analysis for all the components of the end-bearing GC (A_r =25%) stabilized soft soil model.

S. No	Meshing type	Number of elements	Number of nodes
1.	Very coarse mesh	3450	5416
2.	Coarse mesh	4129	6630
3.	Medium mesh	8886	14147
4.	Fine mesh	21133	32530
5.	Very fine mesh	54032	80216

6.3.1 Model test results analysis

The vertical stress-settlement behavior of the single granular column reinforced clay bed was determined through numerical modeling; the results obtained are plotted in Fig. 6.8 – Fig. 6.11. The comparative analysis of the experimental and numerical test results shows that the behavior of the granular column is closely simulated by the finite element model, as depicted in Fig. 6.8. Typical loading-settlement behavior using numerical modeling is depicted in Fig. 6.9 for the plastic granular column. The optimum loading capacity of the floating column was found to be very close to the end-bearing column for an l/d ratio of 8 for the soft soil bed, improved with the non-encased column. Fig. 6.10 and Fig. 6.11 represent the comparative results of the model tests and FEM results for the EGC and EPGC improved soft soils. The utilization of geosynthetic encasement substantially boosts the load-bearing capacity of the composite soil bed, particularly in the case of end-bearing columns, where the increase is notably significant.

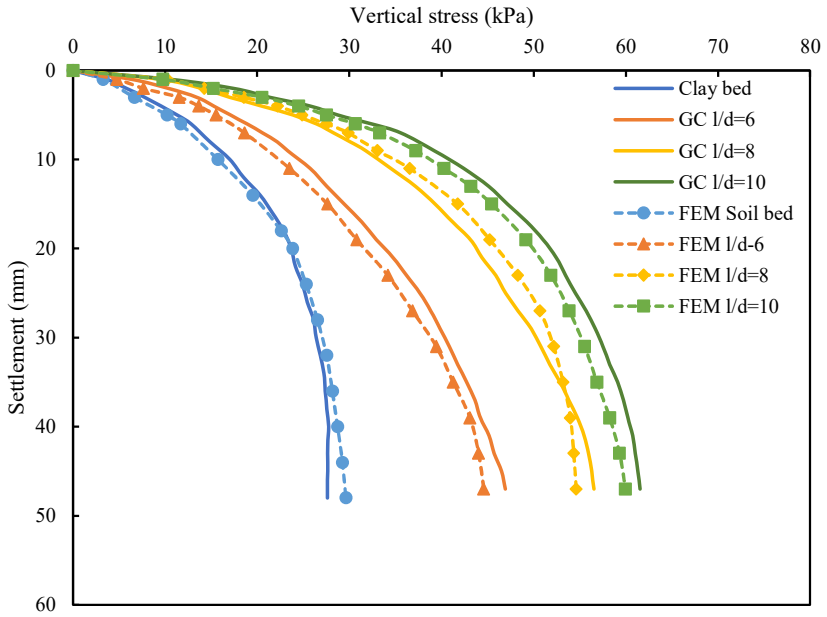

Fig. 6.8 Comparison of numerical model test results with the experimental test results for soft clay bed having Su of 5 kPa improved using GC.

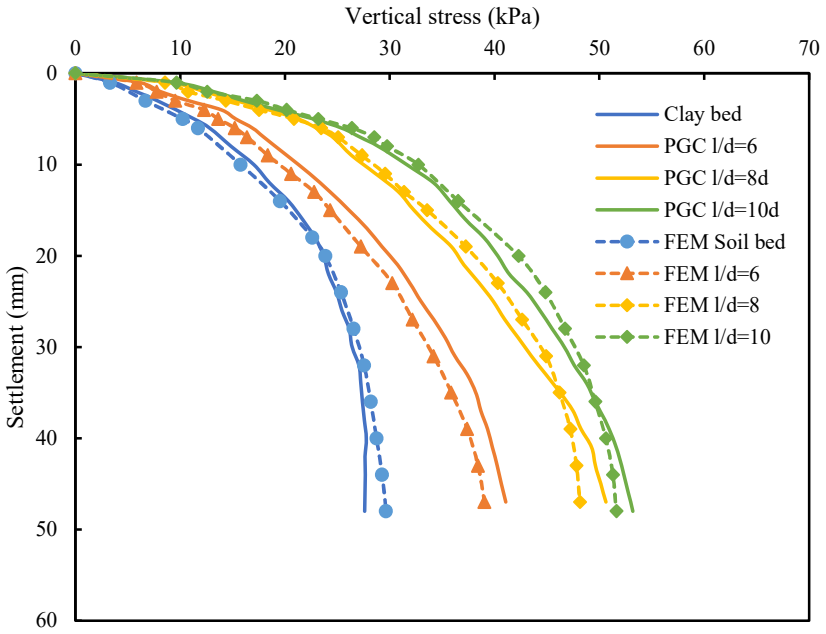

Fig. 6.9 Comparison of numerical model test results with the experimental test results for soft clay bed having Su of 5 kPa improved using PGC.

The composite soil mass undergoes failure by the bulging of the column, as depicted in Fig. 6.12. The column undergoes settlements as well as lateral bulging, which is

evident from the results presented in chapter 4 and here in Fig. 6.12. The use of geosynthetic encasement significantly suppresses the lateral bulging of the column. The lateral bulging of GC and PGC, as well as encased columns determined from the FEM model for soil Su of 5 kPa, is shown in Fig. 6.13. The ultimate loading capacity of the soft clay bed reinforced with non-encased and geogrid encased column determined from the numerical study and the laboratory mode tests is presented in Table 6.3 and 6.4.

Table 6.3 Ultimate stress intensity of GC and PGC reinforced soft clay bed (S_u=5 kPa).

Column configuration	Ultimate loading capacity of the model foundation (kPa)			
	GC		PGC	
	Exp.	FEM	Exp.	FEM
UR	27.65	29.71	27.65	29.71
l/d=6	46.93	44.58	41.07	39.53
l/d=8	56.53	54.61	50.62	48.15
l/d=10	61.72	59.83	53.51	51.62

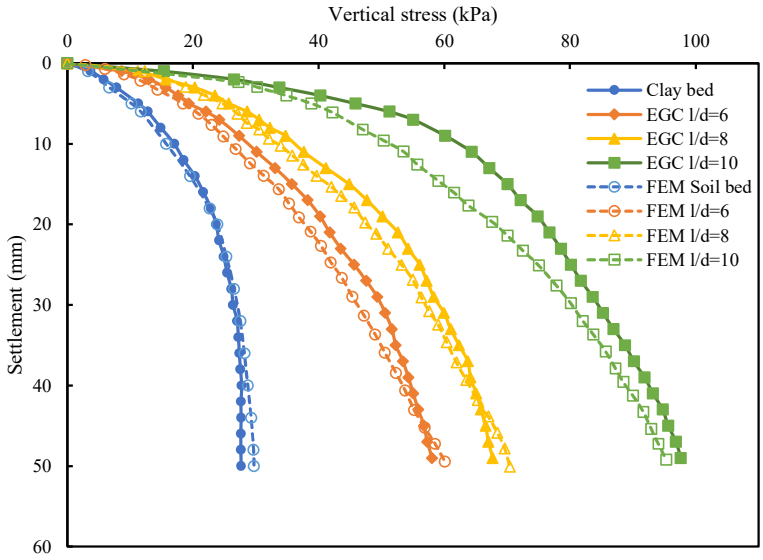

Fig. 6.10 Comparison of numerical model test results with the experimental test results for soft clay bed having Su of 5 kPa improved using EGC.

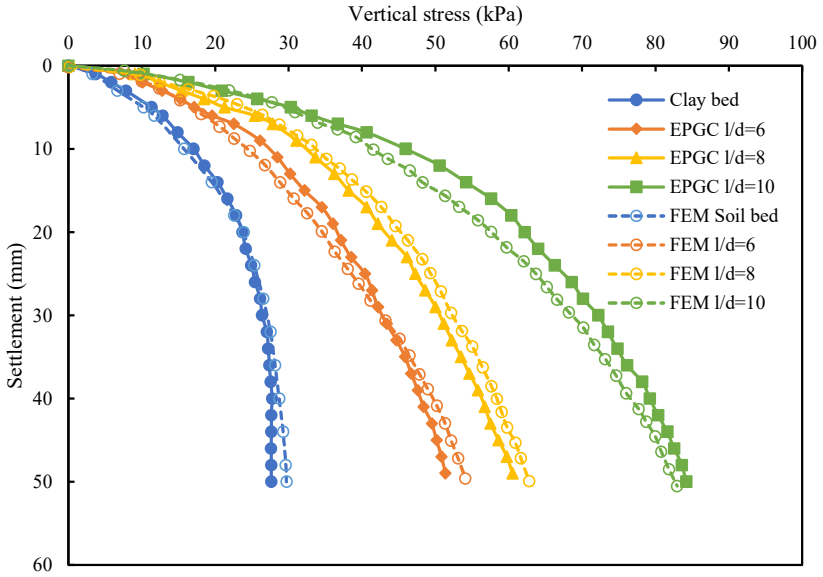

Fig. 6.11 Comparison of numerical model test results with the experimental test results for soft clay bed having Su of 5 kPa improved using EPGC.

Table 6.4 Ultimate stress intensity of GC and PGC reinforced soft clay bed (Su=5 kPa).

Column configuration	Ultimate loading capacity of the model foundation (kPa)			
	EGC		EPGC	
	Exp.	FEM	Exp.	FEM
UR	27.65	29.71	27.65	29.71
l/d=6	58.13	60.07	51.47	54.11
l/d=8	67.70	70.43	60.82	62.80
l/d=10	97.63	95.31	85.32	82.31

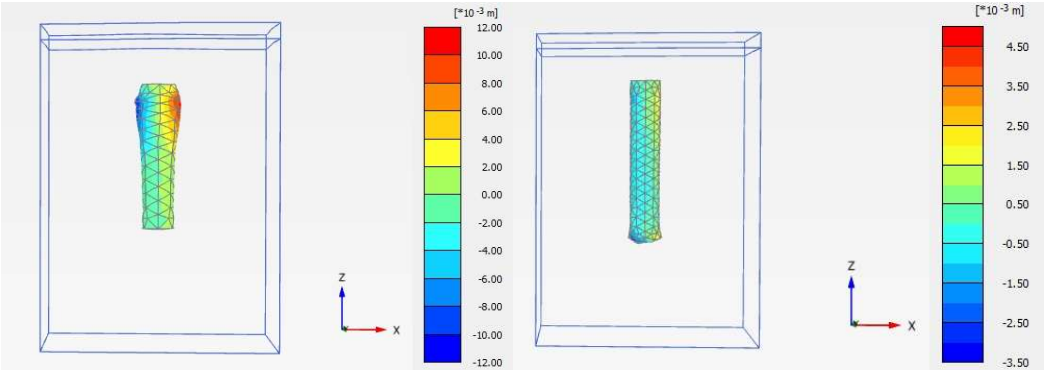

(a) (b)

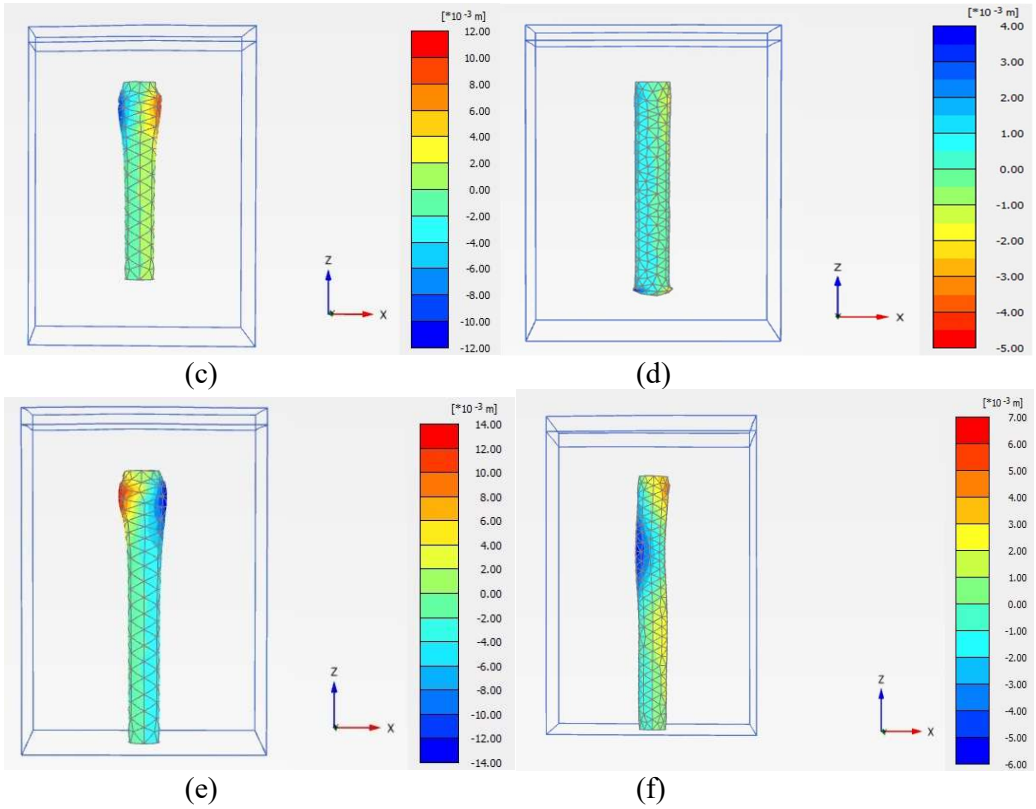

Fig. 6.12 Deformation pattern of the column from numerical analysis: a) GC l/d=6, b) EGC l/d=6, c) GC l/d=8, d) EGC l/d=8, e) GC l/d=10 and f) EGC l/d=10.

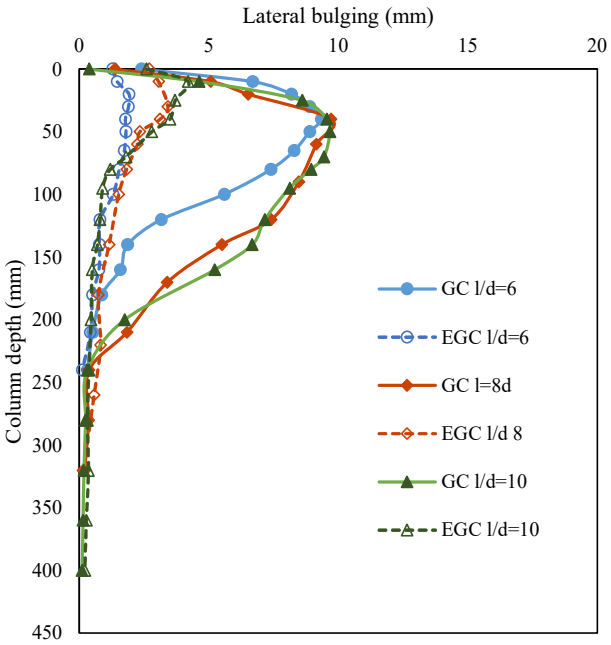

(a)

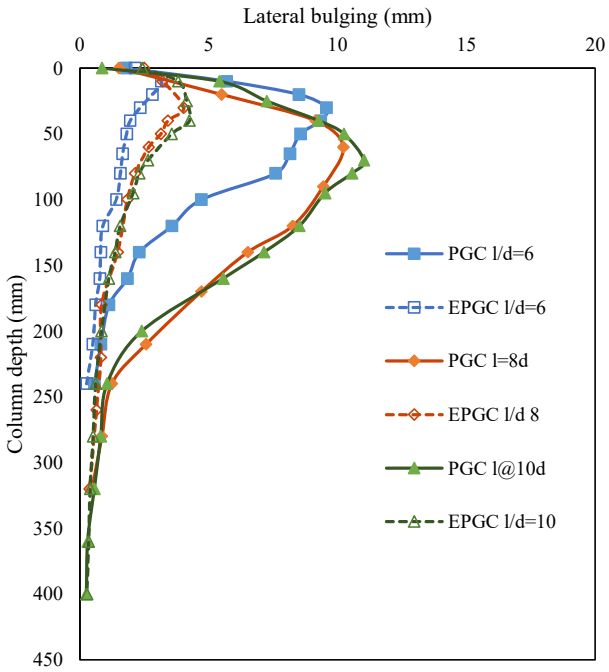

(b)

Fig. 6.13 Lateral bulging of column determined from FEM model for soil bed with S_u of 5kPa: (a) GC and EGC; (b) PGC and EPGC.

6.4 Embankment constructed on the group of GCs reinforced soft soil

In this chapter, numerical modeling of laboratory-constructed embankment model over GCs improved soft soil bed was performed using PLAXIS 3D. Fig. 6.14 shows the model construction and foundation components for the GCs-supported embankment over soft soil. In the present analysis, numerical validation of the embankment over untreated soil bed and a group of end-bearing and floating GCs arranged in a rectangular pattern with an area replacement ratio of 25% is included. The comparisons of applied pressure vs. footing settlement responses measured during the model tests with those predicted by the finite element analyses using PLAXIS 3D under static loading are presented. The mesh sensitivity analysis was carried out in a similar fashion as done for the modeling of single column. The mesh convergence was carried to predict the

settlement of embankment model using mesh size variation from very coarse to very fine by increasing the number of elements as shown in Fig. 6.14.

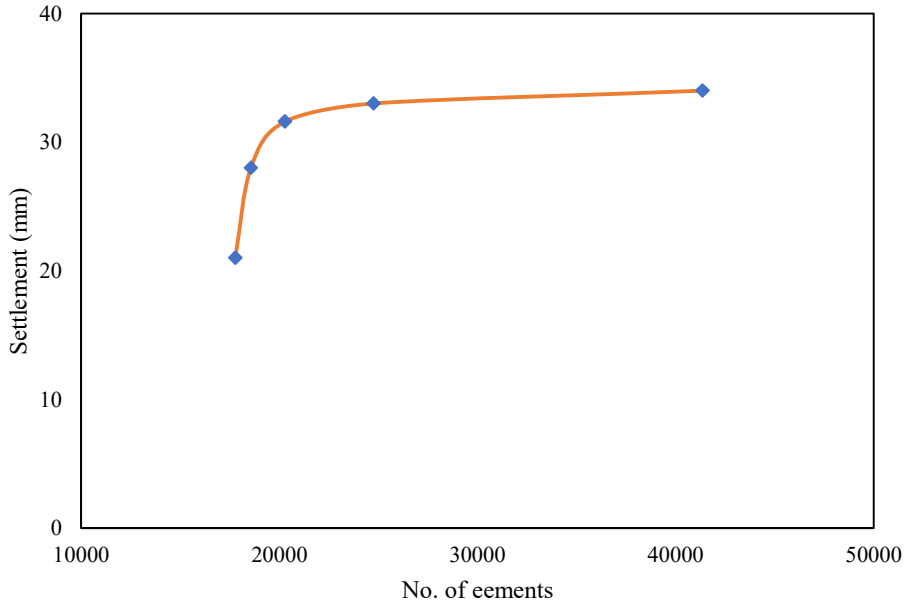

Fig. 6.14 Mesh convergence analysis with the footing settlement for embankment.

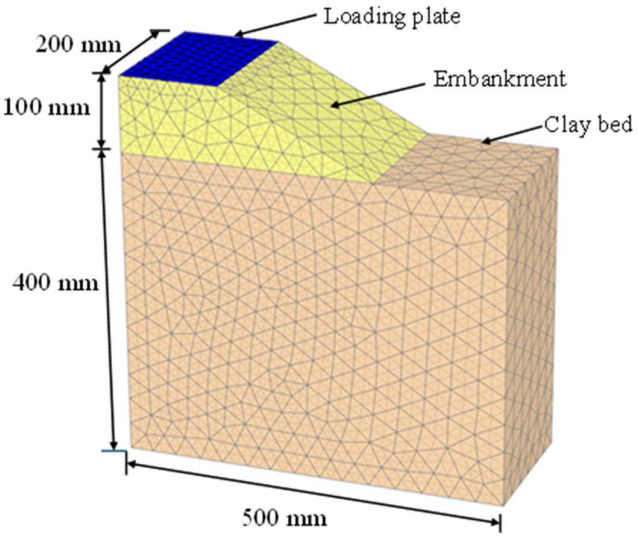

Fig. 6.15 Model creation and mesh generation of embankment in Plaxis 3D.

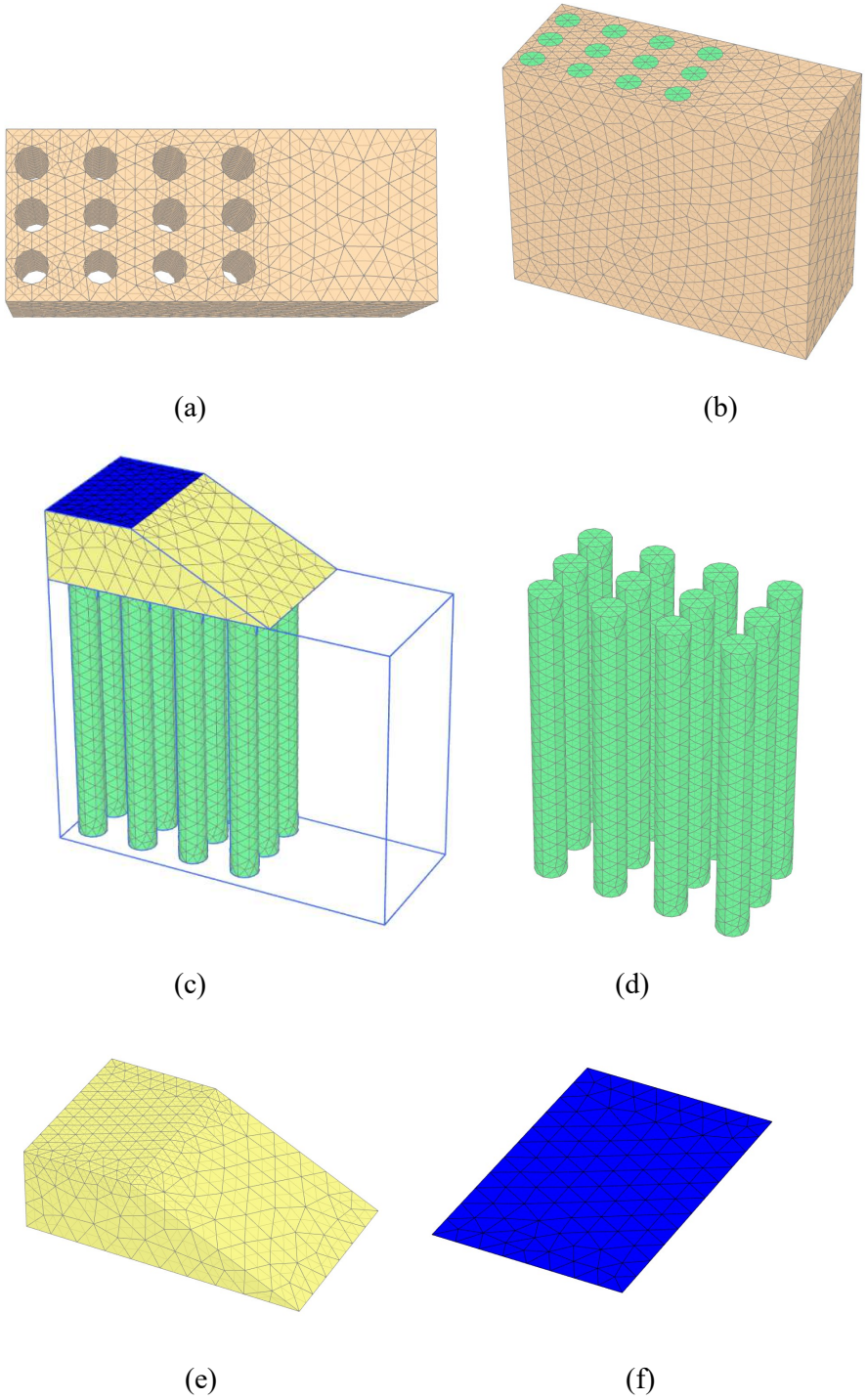

Fig. 6.16 Components of GCs supported embankment on soft soil: (a) Soft soil bed with excavated holes to install GCs, (b) Soft soil bed with a group of GCs, (c) Granular columns positioned in the soil mass, (e) Embankment, (f) Loading plate.

6.4.1 Results of numerical study on Embankment supported by the group of GCs reinforced soft soil

The load intensity-settlement behavior of a group of end-bearing GCs supported embankment for A_r of 25% obtained from laboratory model studies and Plaxis validations is shown in Fig. 6.17 – 6.19. A close agreement is obtained between finite element predictions and measured model test results for the group of GCs supported soft clay under the embankment. The ultimate bearing capacity obtained from the laboratory model tests for the embankment constructed over unreinforced clay bed was found to be 38.34 kPa, and that from numerical analysis was 36.75 kPa at 50 mm of footing settlement, as shown in Fig. 6.17. The ultimate loading capacity of the model embankment supported by floating GCs was observed to be 63.13 kPa, and that obtained from laboratory model tests was 65.53 kPa. This has been depicted in Fig. 6.18. The results of the numerical model test on embankment supported by end-bearing GCs are shown in Fig. 6.19, which is 77.91 kPa compared to 81.26 kPa obtained from the experimental tests. Notably, the validation through Plaxis slightly underestimated the bearing capacity at lower settlements as compared to the laboratory model test results. While the load intensity curve gradually increases with settlement up to 50 mm in the experimental studies, the numerical validation conducted using Plaxis exhibited a similar trend. The vertical and horizontal displacement contours of different components of end-bearing GCs supported embankment on soft soil from finite element analysis at failure under static loading are shown in Fig. 6.20 (a) and (b). It can be observed from the deformation pattern that the columns situated under the loading plate predominantly undergo bulging, whereas the columns located away from the plate exhibit higher lateral movement but less bulging. The vertical and lateral deformation pattern of the embankment supported by a group of floating columns under static

loading is shown in Fig. 6.21. It can be inferred from the figure that floating columns supporting an embankment predominantly undergo vertical deformation with less lateral deformation when compared to end-bearing columns.

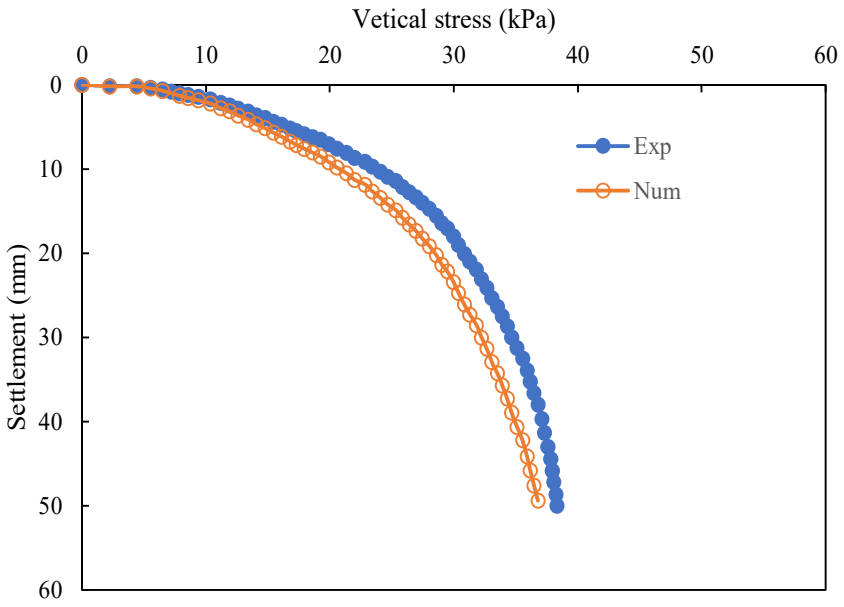

Fig. 6.17 Comparison of measured laboratory model test results with finite element analysis prediction for embankment over soft clay.

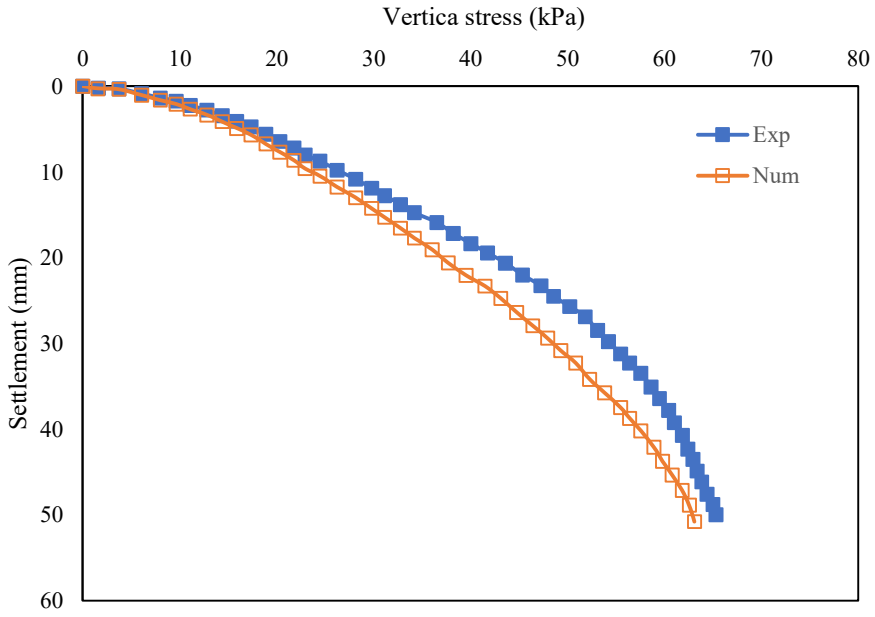

Fig. 6.18 Comparison of measured laboratory model test results with finite element analysis prediction for embankment over soft clay reinforced with floating GCs.

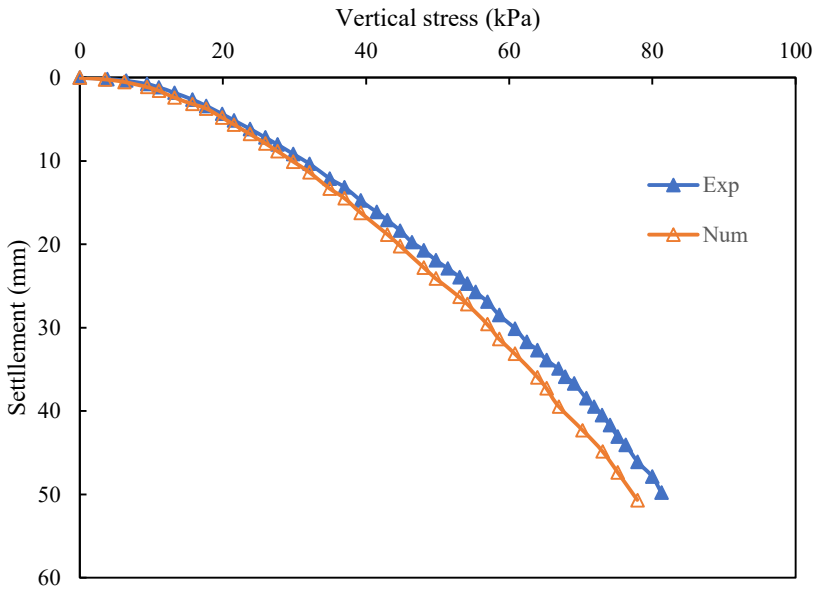

(c)

Fig. 6.19 Comparison of measured laboratory model test results with finite element analysis prediction for embankment over soft clay reinforced with end-bearing GCs.

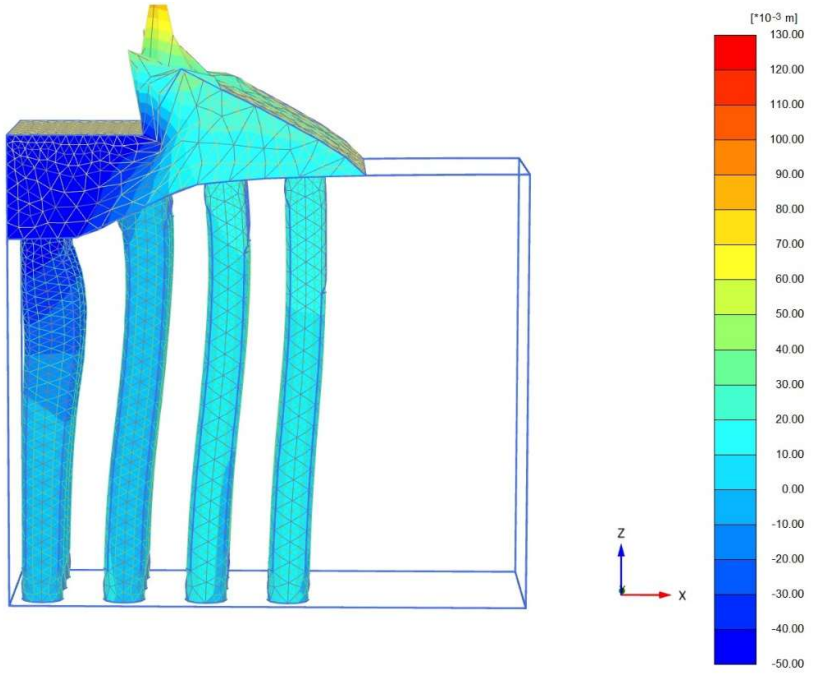

(a)

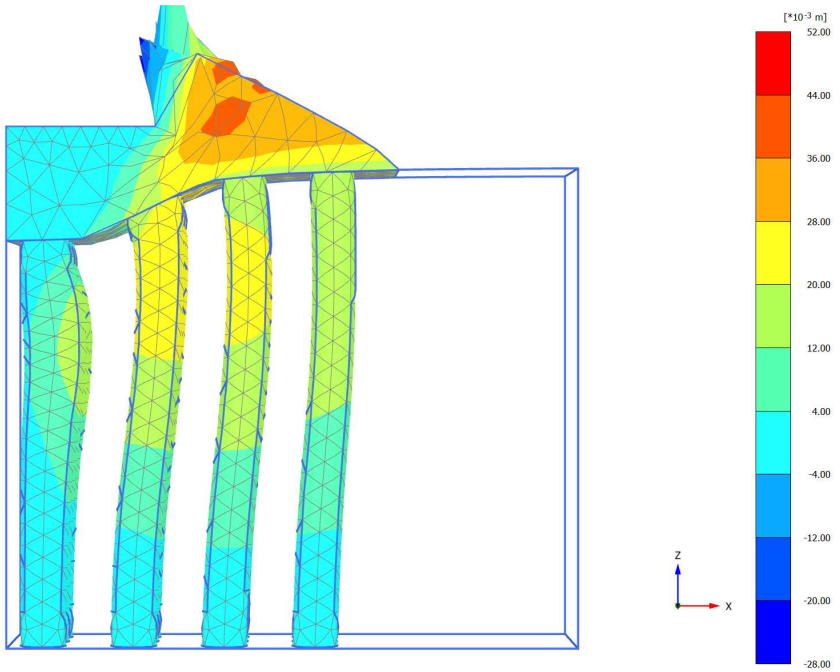

(b)

Fig. 6.20 Displacement contours for different components of end-bearing GCs supported the embankment model at 50 mm footing settlement: (a) Vertical, (b) Lateral.

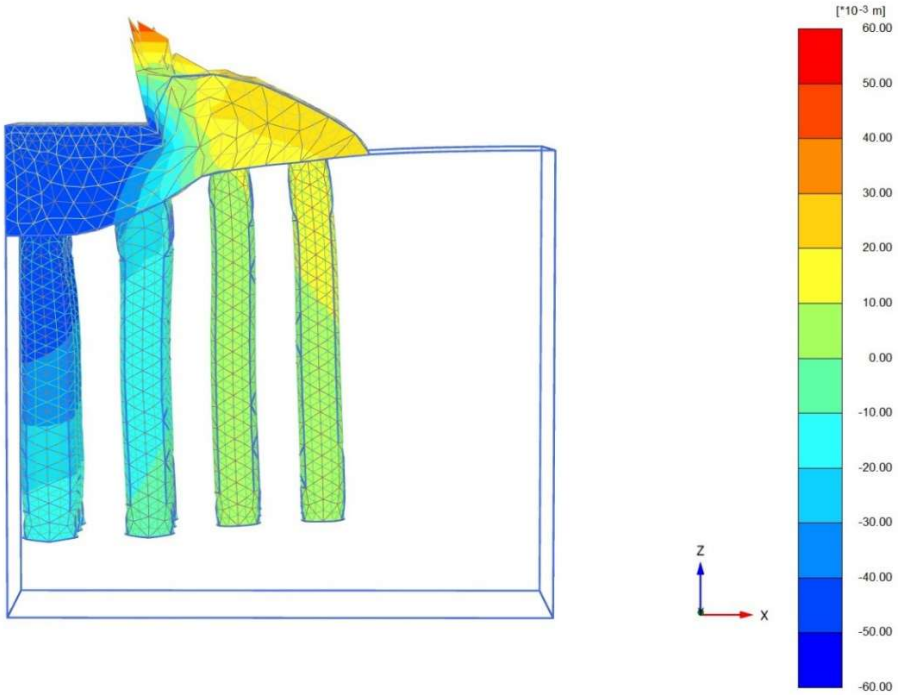

(a)

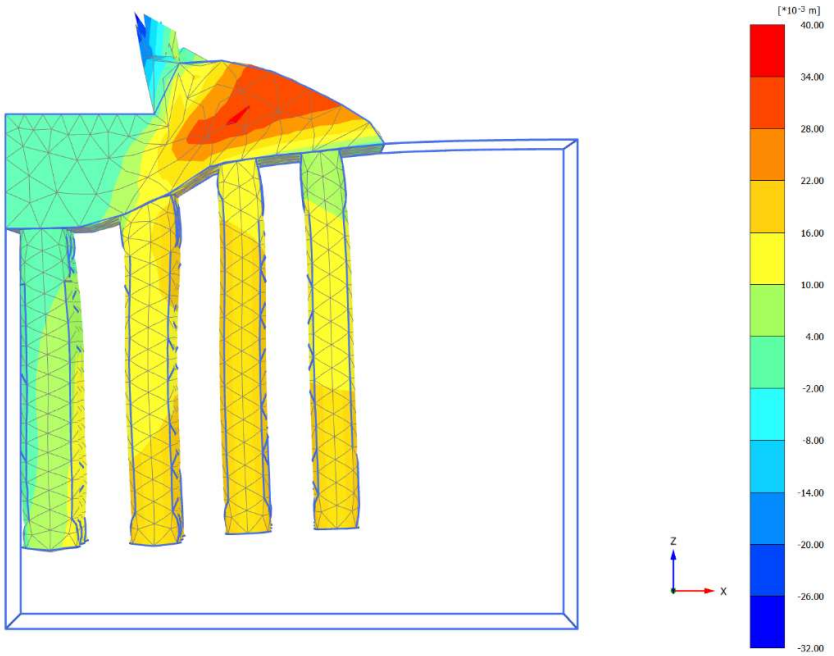

(b)

Fig. 6.21 Displacement contours for different components of end-bearing GCs supported embankment model at 50 mm footing settlement: (a) Vertical, (b) Lateral.

6.5 Conclusion

This chapter discusses the numerical validations of the embankment over end-bearing and floating GCs improved soft soil under static loading conditions. The engineering properties of the soft soil bed, granular column (GC) material, and embankment are determined from laboratory experiments. Three-dimensional, elastoplastic, finite element analyses of GC-supported embankment over soft soil have been conducted using commercially available PLAXIS 3D software. The PLAXIS 3D results regarding vertical stress vs. footing settlement relationship were compared with laboratory model test results from Chapters 4 and 5. The deformation patterns obtained from the numerical modeling closely resemble the embankment and column deformation behavior observed from the experimental study. Both finite element predictions and measured model test results show that end-bearing columns give higher failure stress at lower settlement values

compared to floating columns. Overall, the predicted results from the finite element analyses compare well with the laboratory model test results for the soft ground improved with groups of end-bearing and floating GCs subjected to static loading.